

### A multi-scale multi-physics model of soil drying

L.B. Hu<sup>1,3</sup>, H. Peron<sup>2</sup>, L. Laloui<sup>2</sup> and T. Hueckel<sup>1</sup>, M.ASCE,

<sup>1</sup>Department of Civil and Environmental Engineering, Duke University, P.O. Box 907271, Durham, NC 27708-0287; PH +1(919) 660-5205; FAX (919) 660-5219; email:[hueckel@duke.edu](mailto:hueckel@duke.edu)

<sup>2</sup>Laboratory of Soil Mechanics, Ecole Polytechnique Fédérale de Lausanne, EPFL, Station 18, CH-1015 Lausanne, Switzerland; PH +41 21691 3228, email:[herve.peron@epfl.ch](mailto:herve.peron@epfl.ch); [lyesse.laloui@epfl.ch](mailto:lyesse.laloui@epfl.ch)

<sup>3</sup>currently at Civil and Environmental Engineering, University of Vermont, Burlington, VT 05405, USA; PH (802) 656-4571; Fax: (802)656-8446; email:[Liangbo.Hu@uvm.edu](mailto:Liangbo.Hu@uvm.edu)

#### ABSTRACT

Drying shrinkage is modeled at a microscale as a two-stage process of deformation and evacuation of a two-tube vessel system, based on porosimetry evolution. In the first stage water flow is driven by an external evaporation flux. Flow is associated with a negative pressure (suction) gradient along the vessel. The amount of water evaporated in this stage equals to the vessel volume reduction through the deformation of its walls, as long as the suction constricting the vessel can be supported by water. At some point suction required to further deform the vessel reaches at the vessel exit the water tensile strength. As a result liquid/gas interface penetrates the vessel via undistinguishable mechanisms of meniscus plunging or near-surface cavitation (isothermal evaporation). The subsequent process is modeled as a moving drying front, without much of deformation of the vessels. The resulting macroscopic effective stress is generally compressive due to large suction. However, locally around defects a relatively small tensile total stress is greatly amplified, and hence despite the large suction, the effective stress is tensile and may easily reach tensile strength. Thus, the condition for tensile failure involves microscopic characteristic size of the soil pore system, and its defects.

#### INTRODUCTION

Macroscopic desiccation shrinkage experiments on wet soils indicate that most of the shrinkage during drying occurs while soil is still saturated. Shrinkage stops practically simultaneously with the air entrance into the soil, at the water content (hence referred to as shrinkage limit) still above 20% for the tested soils. The remaining drying process occurs with a much-reduced shrinkage rate, but almost entirely via desaturation (Corte and Higashi, 1964, Fredlund, and Rahardjo, 1993, Konrad and Ayad, 1997, Kodikara et al., 2002). However, specific mechanisms of the shrinkage cessation and air entry are still not well understood. In this context we examine microscopic data of the pore system evolution as represented by the mercury porosimetry results and postulate corresponding mechanisms based on the pressure (suction) development in the vessels and the cavitation.

Experiments with drying (Sherwood, 1929a and b, Peron et al., 2009) show that the process proceeds in at least two stages that are distinctly different, separated by the air

entry value. The event of the air entry is interpreted either as a meniscus plunging or subsurface cavitation in water, which are physically undistinguishable phenomena (Brinker and Scherer, 1990). The former suggest a meniscus shrinking until its diameter is smaller than the pore entrance. The latter, implying that water suction reaches tensile water strength, depends notoriously on the presence of dissolved air or solid impurities in water. The numerical criteria for both events yield the same values of the pore vessel size. In the post air entry stage, evaporation proceeds according to a classical scenario of the receding liquid-vapor interface from the open vessel end, incrementally emptying the filled part of the vessel. This stage is characterized by a marginal water flow, and a minimal vessel deformation, while it is dominated by a displacement of the phase transition interface. The process strongly depends on the vessel size, which controls the liquid pressure at the interface. The model is numerically evaluated, showing an interesting interplay of the deformation of and water loss from the two main pore modes is simulated.

The total stress resulting from the suction in pore vessels depends on the boundary constraints and/or moisture gradients, and often is tensile. However, a high negative pore pressure (suction) leads most commonly to compressive effective stress. This is against the classical physical observation of tensile fractures during drying. However, if the total stress is amplified by a presence of pre-existing flaws at their tip, a tensile effective stress may develop giving rise to fracture. A scenario of desiccation fracture generation, originally proposed by Scherer (1992) for gels is discussed in the context of soil drying.

## MICROSCALE MODEL OF SOIL DRYING

### Deformation and Pore Vessel Flow

The results of the porosimetry performed at three different stages of drying, the onset, near shrinkage limit, and at the nearly complete desaturation are shown in Fig. 1.

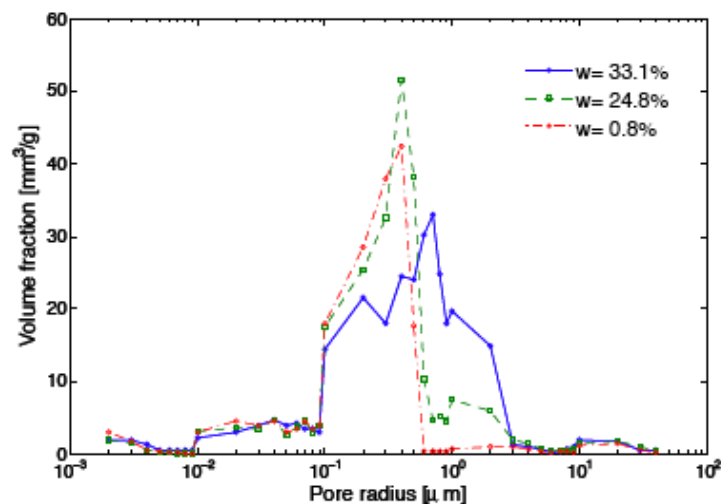


Figure 1. Porosimetry at water content of 33% (liquid limit), 24.8% (shrinkage limit) and near the end of desaturation 0.8%

It can be seen from Fig. 1 that the original (at  $w = 33\%$ ) pores  $> 7 \times 10^{-1} \mu\text{m}$  substantially removed from the medium or transformed at  $w < 24.8\%$ , and altogether disappear at the end of drying (i.e. at  $w = 0.8\%$ ), whereas the volume fraction of the initially smaller pores increases visibly compared to the initial state. To reproduce this evolution, the medium is idealized as consisting from bunches of parallel cylindrical deformable vessels with two initial diameters referred to as Large Pores (LP) of  $1.5 \mu\text{m}$  and respectively, Small Pores (SP) of  $0.5 \mu\text{m}$ , and known elasticity modulus of the solid walls. Given the volume fractions represented in Fig. 1, there is twelve SPs per one LP in a representative volume, shown in Fig. 2a and b, their external wall radius being  $3.6 \mu\text{m}$ . While we discuss only 1-D shrinkage, in a more general case the elementary volumes are arranged as in Fig. 2c with 2-D intercalating layers of tubes oriented orthogonally ones to the others. As a result all quantities are appropriately weighed averages of the values pertaining to individual tubes.

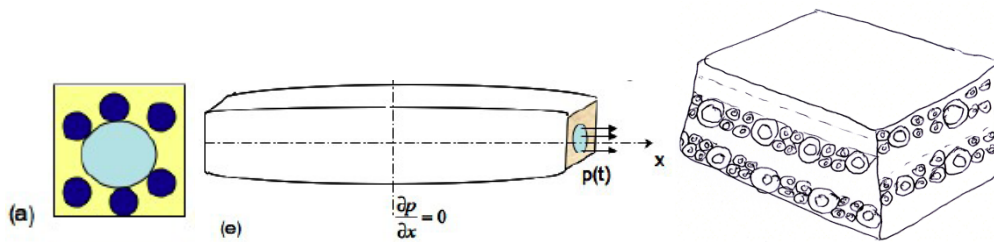


Figure 2. Schematic of arrangement of pore vessels in a representative volume (a) Small and Large pores; (b) single tube and the fluid pressure boundary conditions; (c) orthogonal arrangement of pore vessels.

A linear stress-strain law is adopted for the loading phase, while the unloading (perfectly rigid) is not considered. For the reasons of numerical simplicity, the external perimeter of the tubes is assumed as circular with the equivalent radius of  $3.6 \mu\text{m}$ , calculated in a way to preserve the initial relative volume of solid. The solution for the response of the entire REV has been envisioned as a superposition of solutions for a series of cylindrical vessels with a single cylindrical cavity at the center. These are solutions for one large vessel and for a series of identical small vessels also located centrally. The superposition is admissible because of the geometrical similarity of the BVPs considered and linearity of the stress-strain law. Clearly, the location of all the pores at the center introduces a bias, justified by the randomness of the actual pore distribution. Computationally, the problem is then reduced to that of a single tube with a single cylindrical cavity, to be applied both to LVs and SVs.

Flow through a single vessel is described by (Hu et al., 2010a) in terms of the fluid pressure in the pore-vessel,  $p(x,t)$ ,

$$\frac{\partial^2 p}{\partial x^2} + \frac{2a_0}{Hh \left[ 1 - \frac{a_0 p}{Hh} \right]} \left( \frac{\partial p}{\partial x} \right)^2 - \frac{16\mu}{a_0} \frac{\left[ 1 - \frac{a_0 p}{Hh} \right]}{Hh} \left( \frac{\partial p}{\partial t} \right) = 0 \quad (1)$$

with the boundary conditions  $x = 0, \frac{\partial p}{\partial x} = 0$ ;  $x = L, p = p_0(t)$ .  $2L$  is the length of the tube,  $p_0(t)$  is a pressure exerted at the point of evaporation,  $H$  is inelastic stiffness modulus (1D),  $\mu$  is fluid viscosity,  $h$  is the thickness of the tube,  $a_0$  is the initial radius of the tube at the exit. Equation (1) is a linearized form of the flow equation after Fung (1984), reached under a 1-D flow assumption, and assuming that Poisson ratio is zero. Figures 3a and b show the evolution of the water output for LP and SP in time and along the radius.

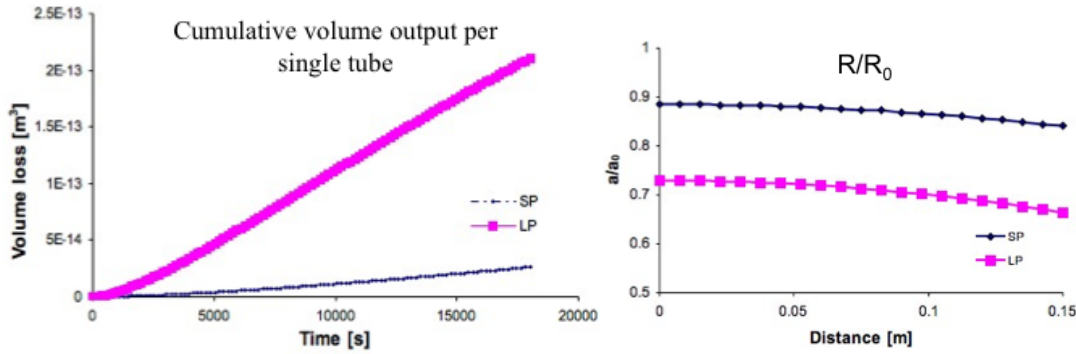


Figure 3. Evolution of water output from the pore vessels (a), and vessel deformation (b).

The pore pressure evolution in Large Pore is shown in Figure 4. It clearly shows that suction in the pore is growing substantially during drying and more pronouncedly at the tube exit.

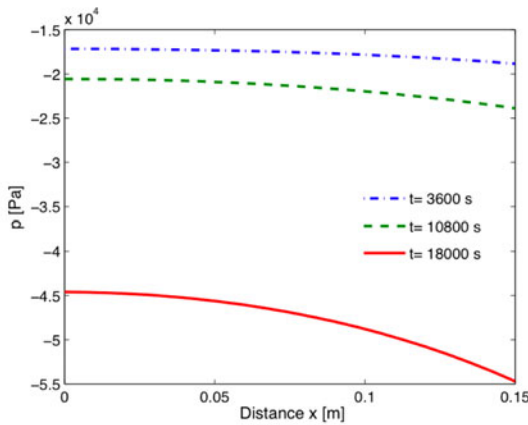


Figure 4. Pore pressure evolution in a Large Pore in the saturated stage

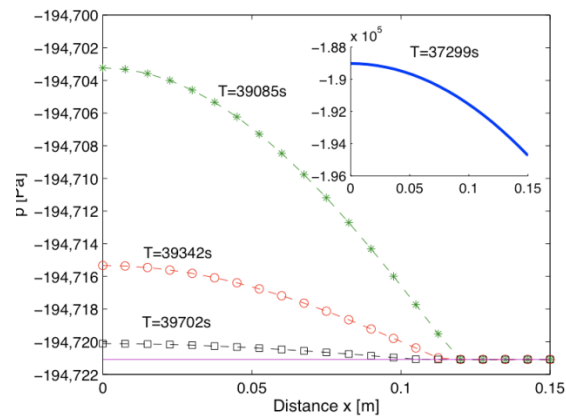


Figure 5. Pressure evolution in the unsaturated stage

### Air Entry and Desaturation Stage

As mentioned before, the increase of suction in the tube water is not unbounded. Water resistance to tension is limited, and while the specific value (known as cavitation pressure) depends on several conditions, it is likely that the limit in soils is rather low. It is believed that cavitation, understood as isothermal evaporation onset forming a bubble

within the water body that eventually becomes unstable. The instability condition of the gas-fluid interface is described by Laplace's law, defined via an equilibrium capillary pressure,  $p_{crit}$ , which depends on the interface curvature radius  $r$ , surface tension  $T_s$ , and contact angle  $\theta$ . The instability occurs near the water free surface where suction is the highest and leads to the air entry. Alternative explanation via a shrinking meniscus plunging into a pore yields numerically the same criterion (Hu et al., 2010a).

$$p_{crit} = -\frac{2T_s \cos \theta}{r} \quad (2)$$

It is postulated that the subsequent incremental removal of vapor from the surface is equivalent to an incremental displacement of the gas/fluid interface within the vessel, denoted  $s(t)$ . Water flow in the remaining portion of the pore-vessel is still Poiseuillian, while the amount of the interface displacement is determined from the mass balance condition, as below

$$\begin{aligned} \frac{\partial p}{\partial t} &= \kappa \frac{\partial^2 p}{\partial x^2}; \quad 0 \leq x \leq s(t) \\ \rho_w \frac{ds}{dt} &= \lambda \frac{\partial p}{\partial x} - \xi \frac{\partial c}{\partial x} \end{aligned} \quad (3)$$

where  $\kappa = Hh_0 a_0 / 16\mu$  can be interpreted as a vessel hydraulic conductivity, whereas  $\lambda = \rho_w a^2 / 8\mu$  is modified Poiseuille constant (to refer to specific mass). The second term of the right hand side of (3b) represents the vapor flux coming out of the interface and entering the gas phase, as  $c$  is the water vapor mass concentration in the gas and  $\xi$  is the diffusion coefficient of the vapor.

The boundary conditions are

$$\begin{aligned} x = s(t) : p &= p_{crit} \\ x = 0 : \frac{\partial p}{\partial x} &= 0 \end{aligned} \quad (4)$$

Gas vapor mixture transport for  $x > s(t)$  is considered as instantaneous and hence ignored.

Fig. 5 shows the evolution of the pore water pressure after the air entry. It may be seen that the evolution breaks down in two stages: the first one with two mechanisms of transport, the second with the only one. Indeed, quite quickly the pressure decreases to zero in the entire tube, and hence the fluid flow ceases. Therefore, the rest of the fluid is subsequently removed in the second stage via displacement of the inter-phase interface.

Both large and small tubes start shrinking in the saturated drying phase at the same time. While the small tubes individually produce a smaller flux, there are 12 of these pores versus one LP, hence their total flux is about half of that effected by the single large tube. The difference in the pore size between LP and SP also uniquely determines the cavitation pressure value at which the two tube types enter the unsaturated tube phase. Clearly, water in SPs cavitates much later than in LPs. Hence, the gaseous phase starts in

SPs at a later stage. An averaging method by combining the volume loss by LPs and SPs gives the estimate of the total volume loss, and hence the void ratio evolution as presented in Fig. 6a and b. The results indicate that a specific sequence of various milestones in the process for each tube, i.e. air entry, cessation of flow and deformation and end of the phase interface motion may yield a different outcome in terms of void ratio evolution. As a consequence, the overall outcome crucially depends on the size of vessels.

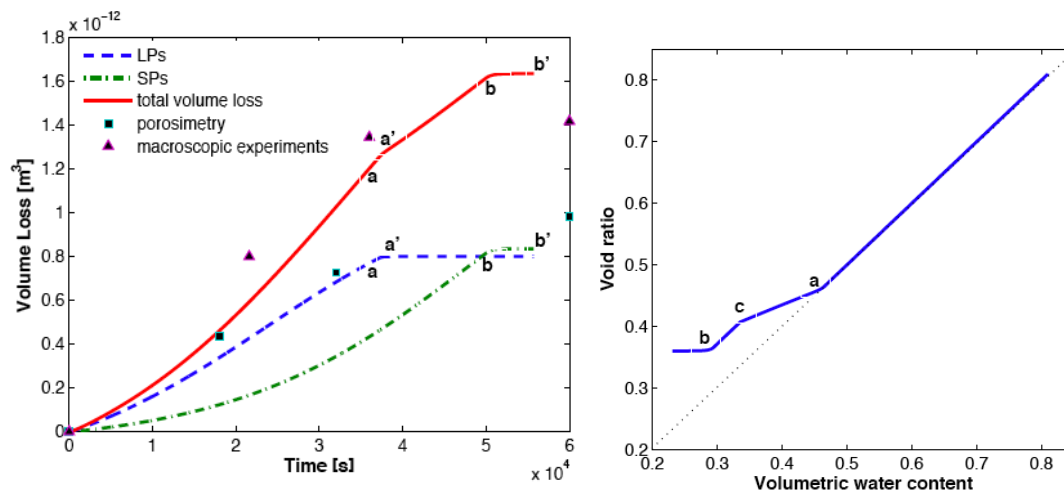


Figure 6. (a) Pore space volume loss evolution during drying with different contributions of LPs and SPs; (b) corresponding void ratio change as a function of the volumetric water content

The distribution of stress components along the radius is illustrated in Fig. 7 both for the case of boundary conditions of free deformation and zero stress at the external tube perimeter, as well as for a case in which the perimeter is constrained. In both cases the circumferential stress is compressive, while radial stress is tensile throughout. The constrained case yields higher stress values, in particular the maximum tensile stress at the inside perimeter is three times higher for the constrained case.

## DESICCATION CRACKING CRITERION

Desiccation macro-cracks are likely to occur if the drying shrinkage is kinematically constrained (Corte and Higashi, 1960). The constraints can arise from several causes (Hueckel, 1992), including: (i) frictional or any other traction or displacement boundary conditions, (ii) any self-equilibrated stress concentrations within the soil sample, and (iii) intrinsic soil inhomogeneity factors, such as soil texture and soil structure, or simply mineral inhomogeneities. In the field, cause (i) may arise from any restraining structure, whereas cause (ii) may occur due to soil moisture gradients, which do not fulfil the strain compatibility conditions.

A fracture mechanism is envisioned as an activation of a pre-existing crack-like micro flaw extending from its surface, at least one order of magnitude larger than a pore size, as proposed by Scherer (1992). A prerequisite of the crack activation is the air entry.

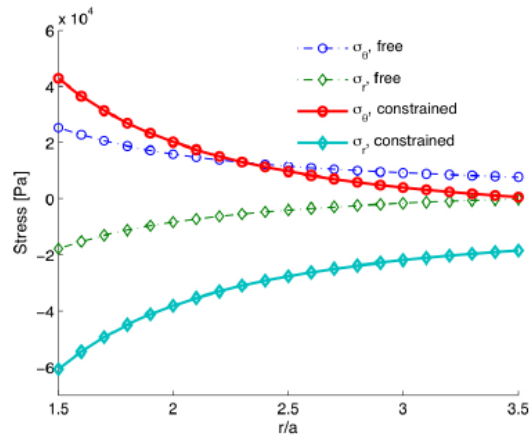


Figure 7. Stress component distribution along the radius at  $t = 18000s$ .

In the stress analysis of drying porous continuum at this scale it is important to strictly distinguish between total stress and effective stress analysis. In the former case, by analogy to thermal cooling, a near surface soil layer is likely to be under tensile total stress induced as a reaction to the constraint of any of the above listed sources. In the case of the constraints induced by a non-uniform water withdrawal during a transient water loss the surface will be under tensile total stress, with a compressed centre. However, when analysing the effective stress in soil mass, one needs to consider the evaporation driven suction in water, which is the highest at the body surface. This suction is usually larger than total tensile stress, producing at the surface the largest effective stress compression. Hence, contrary to a straightforward expectation, tensile cracks would propagate from the compressive zone. This apparent paradox may be resolved by employing a local fracture condition at the tip of a pre-existing flaw (Scherer, 1992).

The main postulate for this condition is that a flaw becomes activated, when it is drained from almost all the water, and filled only at a tip with water under a meniscus of radius  $r_l$ , Figure 8. Therefore, a flaw-face becomes a part of the “external” boundary, at which the conditions for the air entry to the pores are the same as described before. We consider a situation right after the air entry, when the menisci originally of the radius  $r_m > r_p$  in pores, have shrunk to the size of the pores  $r_p = r_m$ , whereas suction (negative pore pressure) is the highest within the body at the location at the external boundary. The macroscopic neighbourhood of the crack is subjected to a tensile total stress, which is a function of the pore water suction (Brinker and Scherer, 1990). However, at the crack tip the acting remotely tensile stress is locally significantly amplified. This is one of the principal findings about the fracture role in stress transmission. Consequently the local total tensile stress at the tip, is much higher than the macroscopic (remote) one. Assuming the plastic field near the tip to be very small and using the effective stress definition, the maximum effective stress at the crack tip induced by a remote total stress  $\sigma_x$  is expressed via a classical finding in fracture mechanics (Cherepanov, 1979)

$$\sigma_c^{rmax} = 2B\sigma_x \sqrt{\frac{c}{r_c}} - p_l \tag{5}$$

where the first term on the RHS of eq. (5) corresponds to the total stress intensity factor,  $c$  is the flaw depth, and  $r_c$  is the radius of the flaw curvature near the tip,  $B = 1.12$  is a constant. Therefore, if the amplifying factor  $\sqrt{(c/r_c)}$  is sufficiently large, the effective stress at the LHS may become tensile despite the fact that the negative pore pressure,  $p$ , is very high.

To cause fracture propagation, according to Scherer's concept, the effective stress near the tip must be high enough to cause fracture of a micro-structural elements with a known strength. For drying soils there are several options to envision a micro-structural failure leading to fracture propagation (Hu, 2008). One of those is related to the constrained case shown before in Fig. 7, with the exception that more realistically, the constraint is imposed at only a limited segment of the external perimeter, where a contact bridge is postulated as for a couple of pore vessels as in Fig. 9, inset a. In such a case the maximum tensile stress occurs at the contact site, and so does failure. In the following considerations for simplicity a constraining contact is assumed to take place between a single-family vessel, and be endowed with a uniaxial tensile strength  $\sigma_{lf}$ . The existing axisymmetric solution (Hu, 2008) clearly does not allow segmental boundary conditions.

Alternatively, Scherer's (1992) technique can be employed, which uses the critical effective stress intensity factor,  $K'_{Icrit}$  to obtain the micro-fracture propagation stress

$$\sigma_c'^{\max} \geq \frac{K'_{Icrit}}{B\sqrt{\pi c'}} \quad (6)$$

where  $K'_{Icrit}$  is replaced in turn by the flaw tip stress, as a remote stress for the micro-flaw. Considering a situation at failure without water pressure, the effective micro-scale intensity factor is expressed via total stress intensity macro-scale factor

$$K'_{Icrit} = 2K_{Icrit}B\sqrt{\frac{c'}{r_c}} \quad (7)$$

or replacing macroscopic stress at the flaw tip with the remote total stress via (5) fracture propagation criterion turns out as follows

$$K_{Icrit} = B\sigma_x\sqrt{\pi c} - \frac{1}{2}p\sqrt{\pi r_c} \quad (8)$$

Given that  $\sqrt{r_c}$  is at least two orders of magnitude smaller than  $\sqrt{c}$ , despite that suction may be an order of magnitude higher than the total remote stress, it is possible to express the microscopic local fracture propagation condition due to drying in terms a macroscopic total stress as follows

$$\sigma_x = \frac{K_{Icrit}}{B\sqrt{\pi c}} \quad (9)$$

Peron (2008) has simulated constrained drying slab experiments on Bioley silt by applying suction corresponding to water contents. At the point when  $w = 22\%$  corresponding to experimentally observed cracking, the simulated effective stress was 44 kPa at 100 kPa suction, yielding a tensile total stress of -56 kPa.

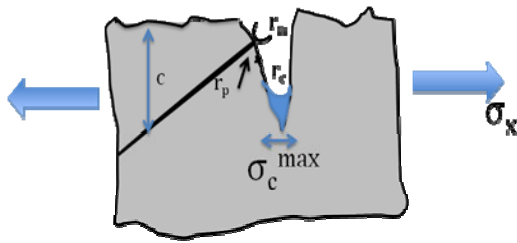


Figure 8. Stress concentration near a flaw tip filled right after the air entry point.

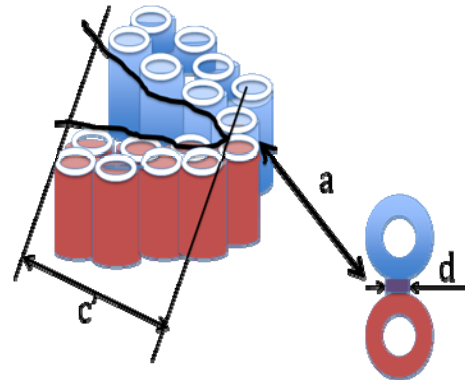


Figure 9. A micro-flaw of a depth  $c'$  in a system of pore vessels propagating incrementally over a distance  $d$ .

Assuming a flaw depth equivalent to 4 (external) pore-vessel diameters  $4 \times 3.6 \mu\text{m} = 0.014 \text{ mm}$  one can estimate  $K_{I \text{ crit}}$  for Bioley silt to be of the order of magnitude of  $0.41 \text{ kNm}^{3/2}$ . For a much more significant flaw of 20 pore-vessel diameters of  $3.6 \mu\text{m}$  equal to  $0.072 \text{ mm}$  eq. (9) yields  $K_{I \text{ crit}} = 0.94 \text{ kNm}^{-3/2}$ . The above results are consistent with other measurements for silts using ASTM method yielding values consistently below  $K_{I \text{ crit}} = 1 \text{ kNm}^{-3/2}$  (see e.g. Lakshmikantha et al., 2008).

## CONCLUSIONS

The presented, largely micro-scale study of soil drying is based on the actual data concerning the evolution of pore structure during drying, and a very geometrically simplified, but physically complex, numerical model and simulations. The model identifies a sequence of milestones in the behavior of soil during drying, and relates them to the pore structure evolution. It appears that the intense shrinkage stage of drying corresponds to an outflow of liquid water from largest size pore vessels and its evaporation at the external drying body surface. The pore vessel constriction induces most of the body shrinkage. Also the largest pore vessels are the first to experience the air entry, when their ability to constrict decreases with deformation. As the air entry criterion a limiting surface tension force value is used. The unsaturated stage of drying is modeled initially, as a Poiseuille flow in the wet portion of the larger pore vessels, and in smaller pore vessels, and the water/air interface progressive penetration inside of the larger vessels leaving the air filled vessel portion unstressed. The smaller are the Small Vessels, the higher is the suction. A schematic characteristic curve has been reconstructed quite realistically, as well as the evolution of the soil porosity as a function of water content. The desiccation cracking criterion developed at a macro-scale level) yields (for Bioley silt)  $K_{I \text{ crit}} = 0.94 \text{ kNm}^{-3/2}$  which is a realistic value.

## ACKNOWLEDGEMENTS

This work was funded by the US NSF, grant # 0324543 and Swiss NSF, grant # 200021-101917.

## REFERENCES

- Brinker, C.J. and Scherer, G.W. 1990. *Sol-Gel Science*, Academic Press, Boston.
- Cherepanov, G.P., 1979. *Mechanics of Brittle Fracture*, McGraw-Hill, New York.
- Fredlund, D.G., and Rahardjo, H. 1993. *Soil Mechanics for Unsaturated Soils*. Wiley
- Fung, Y.C. 1984, *Biodynamics: Circulation*. New York: Springer.
- Hu, L.B., 2008. *Physico-Chemo-Mechanical Coupling Mechanisms in Soil Behavior*, Ph.D. Thesis, Duke University.
- Hu, L.B., Peron, H. Hueckel, T., Laloui, L. 2010a. Desiccation Shrinkage of Non-clayey Soils. Part 1: Concepts and a Microstructural Model, *Computers and Geotechnics*, submitted.
- Hu, L.B., Peron, H. Hueckel, T., Laloui, L. 2010b. Desiccation Shrinkage of Non-clayey Soils. Part 2: A numerical Study, *Computers and Geotechnics*, submitted.
- Hueckel, T. 1992. Water-mineral interaction in hygromechanics of clays exposed to environmental loads: a mixture-theory approach. *Canadian Geotechnical Journal*, 29: 1071-1086.
- Hueckel, T., and Pellegrini, R., 1992. Effective Stress And Water-Pressure In Saturated Clays During Heating-Cooling Cycles, *Canadian Geotechnical J.*, 29, 6, 1095-1102.
- Kodikara, J., Barbour, S.L., and Fredlund, D.G. 2002. Structural development in surficial heavy clay soil: a synthesis of mechanisms. *Australian Geomechanics J.*, 37(3): 25-40.
- Konrad, J.M., and Ayad, R. 1997. An idealized framework for the analysis of cohesive soils undergoing desiccation. *Canadian Geotechnical J.*, 34: 477-488.
- Lakshmikantha, M.R., Prat, P.C., Tapia, J., Ledesma, A. 2008. Effect of moisture content on tensile strength and fracture toughness of a silty soil, *Unsaturated Soils: Advances in Geo-Engineering*, Toll et al. (eds), Taylor & Francis Group, London.
- Peron, H., 2008. *Desiccation cracking of soils*, Ph.D. Thesis, Ecole Polytechnique Federal de Lausanne, Lausanne, Switzerland.
- Peron, H., Laloui, L., Hueckel, T., Hu, L.B. 2009, Fundamentals of desiccation cracking of fine-grained soils: experimental characterisation and mechanisms identification. *Canadian Geotechnical Journal*; 46(10):1177- 1201.
- Pickard, W.F. 1981. The ascent of sap in plants. *Progress in Biophysics and Molecular Biology*; 37(3):181-229.
- Scherer, G.W., 1992. Crack-tip stress in gels, *J. of Non-Crystalline Solids*, 144, 210-216.
- Sherwood, T.K. 1929. The drying of solids - I. *Industrial and Engineering Chemistry*; 21(1):12-16.
- Sherwood, T.K. 1929. The drying of solids - II. *Industrial and Engineering Chemistry*; 21(10):976-980.